CMS Physics Analysis Summary

Contact: cms-pag-conveners-top@cern.ch 2020/03/12

Measurement of differential cross sections for single top quark production in association with a W boson at $\sqrt{s} = 13$ TeV

The CMS Collaboration

Abstract

Measurements are presented of normalized differential cross sections for the production of single top quarks in association with a W boson, in proton-proton collisions at a centre-of-mass energy of 13 TeV. Events containing one muon and one electron in the final state are analyzed. A fiducial region is defined according to the detector acceptance, and the requirement of exactly one b-tagged jet. The presence of lower-energy jets is vetoed to reduce the contribution from backgrounds. The resulting distributions are unfolded to particle-level and compared with predictions calculations at next-to-leading order in perturbative QCD. Within current uncertainties, all the predictions agree with the data.

1 Introduction

Electroweak production of top quarks was first observed by the D0 [1] and CDF [2] Collaborations at the Fermilab Tevatron. At leading order (LO), single top quarks are produced via three processes: the exchange of a virtual W boson (t channel), the production and decay of a virtual W boson (s channel), and the associated production of a top quark and a W boson (tW channel). The latter, which has a negligible production cross section in proton-antiproton collisions at the Tevatron, represents a significant contribution to single top quark production in proton-proton (pp) collisions at the CERN LHC. The study of the tW process does not only provide a unique opportunity to further understand the standard model (SM) and its extensions through the interference of the process at next-to-leading order (NLO) with top quark pair ($\mathrm{t\bar{t}}$) production [3–5], it also plays an important role because of its sensitivity to physics beyond the SM [6–8].

The cross section for tW production has been computed to approximate next-to-next-to-leading order (NNLO) [9]. The theoretical prediction in pp collisions at $\sqrt{s} = 13\,\text{TeV}$, for a top quark mass ($m_\mathrm{t}$) of 172.5 GeV, is $\sigma_\mathrm{tW} = 71.7 \pm 1.8\,(\text{scale}) \pm 3.4\,(\text{PDF})\,\text{pb}$. The first uncertainty refers to the factorization (μ_F) and renormalization (μ_R) scales in quantum chromodynamics (QCD), and the second to parton distribution functions (PDFs). This value includes the charge-conjugate modes. The LO Feynman diagrams for tW production are shown in Fig. 1.

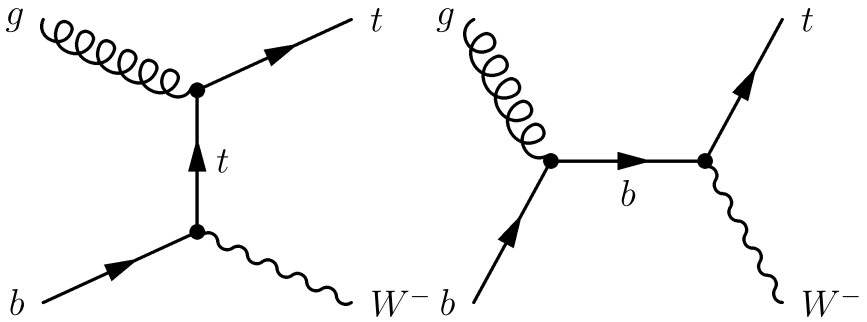

Figure 1: Leading order Feynman diagrams for single top quark production in the tW mode. The charge-conjugate modes are implicitly included.

The CMS and ATLAS Collaborations have presented evidence for [10, 11] and observation of [12, 13] this process in pp collisions at $\sqrt{s} = 7$ and 8 TeV, respectively. Using 13 TeV data, the inclusive tW production cross section has been measured by both collaborations [14, 15] with a precision of the order of 10% and 30%, respectively.

The measurement of the differential cross sections is particularly challenging because of the overwhelming presence of $\mathrm{t\bar{t}}$ events in the most signal-enriched region. The first measurement of the differential cross section of the tW production process was performed by the ATLAS Collaboration [16], using a cut-based analysis in a signal-enriched region defined by a cut on a multivariate discriminant. The measurement reported in this note uses data recorded in 2016, corresponding to an integrated luminosity ($\mathcal{L}$) of $35.9 \pm 0.9\,\text{fb}^{-1}$. The analysis is performed using the $\mathrm{e}^{\pm}\mu^{\mp}$ dilepton channel, in which both W bosons, either produced in association with the top quark or from the decay of the top quark, decay leptonically into a muon or an electron, and a neutrino. Events with W bosons decaying into τ leptons, that decay into electrons or muons, also contribute to the measurement. The primary background to tW production in this final state comes from $\mathrm{t\bar{t}}$ production, with Drell–Yan (DY) production of τ lepton pairs that decay leptonically being the next most significant background. The measurement is performed in a fiducial region in which the signal process is enriched. The results, that are compared with several predictions, are obtained as a function of the following observables:

- the transverse momentum (p_{T}) of the leading (highest p_{T}) lepton,
- the jet p_{T},
- the difference in the ϕ angle of the muon and the electron, $\Delta\varphi(\mathrm{e}^{\pm}, \mu^{\mp})$;
- the longitudinal momentum component of the system formed by the muon, the electron and the jet of the event, $p_{\mathrm{Z}}(\mathrm{e}^{\pm}, \mu^{\mp}, j)$;
- the invariant mass of the system formed by the electron, the muon and the jet, $m(\mathrm{e}^{\pm}, \mu^{\mp}, j)$;
- the transverse mass of the system formed by the electron, the muon, the jet and the missing transverse momentum, $m_{\mathrm{T}}(\mathrm{e}^{\pm}, \mu^{\mp}, j, p_{\mathrm{T}}^{\mathrm{miss}})$.

The first two variables provide central information regarding the kinematic properties of the events. In addition, they provide another means of modeling the top quark p_{T}. The $\Delta\varphi(\mathrm{e}^{\pm}, \mu^{\mp})$ variable allows the exploration of correlations between both physical objects and exploring spin-related properties. The $p_{\mathrm{Z}}(\mathrm{e}^{\pm}, \mu^{\mp}, j)$ distribution can be used to probe the boost of the complete tW system. The last two, invariant and transverse mass, permit to study mass/energy related properties of the whole system.

This document is structured as follows. Section 2 gives a summary of the Monte Carlo (MC) event simulation used. The object and event selection criteria are discussed in Section 3. The information regarding the signal extraction as well as the unfolding performed is given in Section 4. The sources of systematic uncertainties taken into account are described in Section 5. The results are discussed in Section 6, and a summary of the results is presented in Section 7.

2 Monte Carlo simulation

The tW signal is simulated at NLO using POWHEG v1 [17] with the NNPDF 3.0 PDF set [18], and PYTHIA v8.205 [19] is used for parton showering and hadronization. The definition of tW production in perturbative QCD mixes with $\mathrm{t\bar{t}}$ production at NLO [3–5]. Two schemes are proposed to describe the tW signal and to take into account this interference: "diagram removal" (DR) [3], where all NLO diagrams which are doubly resonant, such as those in Fig. 2, are excluded from the signal definition; and "diagram subtraction" (DS) [3, 20], in which the differential cross section is modified with a gauge-invariant subtraction term, that locally cancels the contributions from $\mathrm{t\bar{t}}$ diagrams. In order to compare the results with expectations from theory, a sample of the tW process generated at NLO with MADGRAPH5_aMC@NLO v2.2.2 [21], DR, and NNPDF 3.0 PDFs, interfaced with PYTHIA v8.205 is also provided.

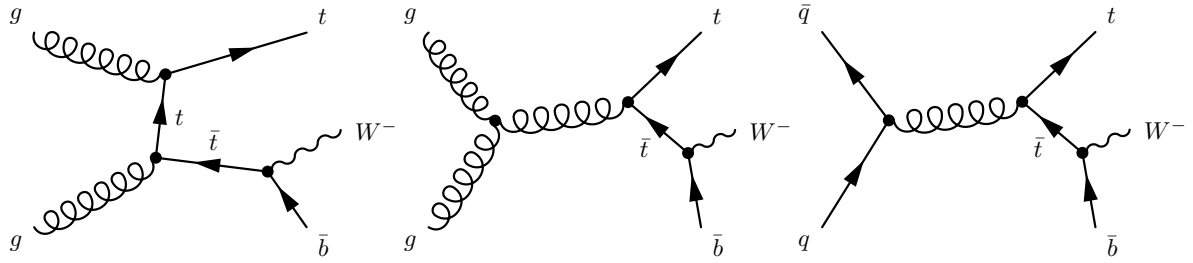

Figure 2: Feynman diagrams for tW single top quark production at NLO that are removed from the signal definition in the DR scheme, the charge-conjugate modes are implicitly included.

The NLO POWHEG v2 [22] setup is used to simulate $\mathrm{t\bar{t}}$ events, as well as the dependency of the $\mathrm{t\bar{t}}$ production on μ_{R} and μ_{F}, and the PDF set. The NNPDF 3.0 set is used as the default PDF set. Parton showering and hadronization for the $\mathrm{t\bar{t}}$ events are handled by PYTHIA v8.205. Other

background contributions are also estimated from MC simulations. The DY and W+jets background samples are generated at NLO with MADGRAPH5_aMC@NLO v2.2.2 [21] with NNPDF 3.0 PDFs, interfaced with PYTHIA v8.205. These processes are simulated with up to two additional partons and the FxFx scheme [23] is used for the merging. The contributions from WW, WZ, and ZZ (referred to as VV) processes are simulated at LO with PYTHIA v8.205. Other contributions from W and Z boson production in association with $\mathrm{t\bar{t}}$ events (referred to as $\mathrm{t\bar{t}V}$) are simulated at NLO using MADGRAPH5_aMC@NLO v2.2.2 and interfaced with PYTHIA v8.205. For all the processes except for $\mathrm{t\bar{t}}$, the underlying event tune CUETP8M1 [24, 25] is used. For $\mathrm{t\bar{t}}$ events the underlying event tune CUETP8M2T4 [26] is utilized. Finally, lepton+jets events in the $\mathrm{t\bar{t}}$ and W+jets samples described above are used to estimate the contribution to the background from events with a jet incorrectly reconstructed as a lepton or with a lepton incorrectly identified as being isolated. As these last contributions to the background contain a lepton candidate that does not originate from a leptonic decay of a gauge boson, they are labeled non-W/Z.

To compare with the observed distributions, the event yields in the simulated samples are normalized to $\mathcal{L}$ using their theoretical cross sections. These are taken from NNLO for W+jets and DY [27], approximate NNLO for tW events [9], and NLO calculations for diboson [28]. For the simulated $\mathrm{t\bar{t}}$ sample, the full NNLO plus next-to-next-to-leading-logarithmic accuracy calculation [29], performed with the TOP++ 2.0 program [30], is used. The PDF uncertainty is added in quadrature to the uncertainty associated with the strong coupling constant (α_S) to obtain a $\mathrm{t\bar{t}}$ production cross section of $832\,^{+20}_{-29}\,(\text{scale}) \pm 35\,(\text{PDF}+\alpha_S)$ pb assuming $m_\mathrm{t} = 172.5\,\text{GeV}$. The simulated samples include additional interactions per bunch crossing (pileup), with the distribution matching that observed in data, with an average of 23 collisions per bunch crossing.

Measurements of the differential cross section for top quark pair production have shown that the transverse momentum of the top quark is softer than predicted by the POWHEG simulation [31, 32]. In order to better model the main background, the effect of this mismodeling of the p_T spectrum is corrected by reweighting the $\mathrm{t\bar{t}}$ simulation to that measured in the data. The factors used for this reweighting are extracted from data using differential measurements at parton level in events with one or two leptons [32–35] and comparing them with respect to the NLO theory predictions from POWHEG.

3 Event selection

In the SM, top quarks decay almost 100% of the time into a W boson and a bottom quark. The analysis described here uses events in the $\mathrm{e}^{\pm}\mu^{\mp}$ final state, in which the W boson from the decay of the top quark and the W boson produced in association with the top quark both decay leptonically, one into an electron and a neutrino, and the other into a muon and a neutrino. This leads to a final state composed of two leptons with opposite charge, one jet resulting from the fragmentation of a bottom quark, and two neutrinos. The event selection used here follows closely that used in the measurement of the inclusive production cross section for single top quarks in association with W bosons [14]. Therefore, only basic requirements are given hereafter (a more detailed description can be found in Ref. [14]).

Events are required to pass either a dilepton or a single-lepton trigger. The particle-flow (PF) algorithm [36] attempts to reconstruct and identify each individual particle in an event with an optimized combination of information from the various elements of the CMS detector. Leptons (electrons [37] or muons [38]) in the event are required to be well isolated and to have $p_\mathrm{T} > 20\,\text{GeV}$ and $|\eta| < 2.4$. Electron candidates in the transition region between the barrel and endcap calorimeters, corresponding to $1.4442 < |\eta| < 1.5660$, are rejected because the re-

construction of electrons in this region is not optimal. Events with W bosons decaying into τ leptons are considered as signal only if the τ leptons decay into electrons or muons that satisfy the selection requirements. In events with more than two leptons passing the selection, the two with the largest p_T are kept for further study. Jets are reconstructed from the PF candidates using the anti-k_T clustering algorithm [39, 40] with a distance parameter of 0.4. Jet energy corrections, derived from simulation, are applied so that the average response to jets matches the particle-level jets [41]. In situ measurements of the momentum balance in dijet, photon+jet, Z+jet, and multijet events are used to account for residual differences in jet energy scale (JES) between data and simulation. Jets are required to have $p_T > 30\,\text{GeV}$ and $|\eta| < 2.4$. Jets passing the above identification criteria but with p_T between 20 and 30 GeV are referred to as "loose jets". The missing transverse momentum vector $\vec{p}_T^{\,\text{miss}}$ is defined as the negative vector sum of the momenta of all reconstructed PF candidates in an event, projected onto the plane perpendicular to the direction of the beam axis. Its magnitude is referred to as p_T^{miss} and the corrections to jet momenta are propagated to the p_T^{miss} calculation [42]. Jets are identified as b jets using the combined secondary vertex algorithm v2 [43], with an operating point that yields identification efficiencies of ≈70% and misidentification (mistag) probabilities of about 1% and 15% [43] for light-flavor jets (u, d, s, and gluons) and c jets, respectively, as estimated from simulated events.

Events are selected as belonging to the $e^{\pm}\mu^{\mp}$ final state if the two leptons with largest p_T passing the above selection criteria are an electron and a muon of opposite charge. The leading lepton is required to have $p_T > 25\,\text{GeV}$. To reduce the contamination from DY production of τ lepton pairs with low invariant dilepton mass, the invariant mass of the lepton pair is required to be greater than 20 GeV. Remaining events are classified according to the number of jets and identified b jets in the event. The most signal-enriched region is the one with one jet that is tagged as a bottom jet (1j1b region), but the size of the signal in comparison with the overwhelming $t\bar{t}$ background is still tiny. An additional selection criteria with respect to Ref. [14] is applied to enhance the signal-to-background ratio. Figure 3 shows the distribution of the number of loose jets in the events in the 1j1b region, as well as the number of jets and b-tagged jets in the $e^{\pm}\mu^{\mp}$ channel. The signal-to-background ratio is higher for events with zero loose jets. Therefore, to minimize the relative contribution from the $t\bar{t}$ background, the signal region is defined as that with events in the 1j1b region and without loose jets. The distributions of the variables under consideration for data and simulated events in the signal region are shown in Fig. 4.

4 Measurement of the differential cross section

In order to take into account the migration of events among the bins of the differential distributions and outside the fiducial phase space produced by the detector response when extrapolating the results to the fiducial phase space defined by particle-level objects, unfolding techniques are used to calculate the differential cross section. For each measured variable, the response matrix (R) parameterizing the migrations among bins is constructed using the signal MC simulations. The number of signal events in the bins of the unfolded distribution ($N_j^{\text{sig, unf}}$) can be estimated following this expression

$$N_i^{\text{sig}} = N_i - N_i^{\text{bkg}} = \sum_{j=1} R_{ij} N_j^{\text{sig, unf}}, \tag{1}$$

where N_i^{sig} is the number of signal events in bin i at detector-level, N_i is the number of observed

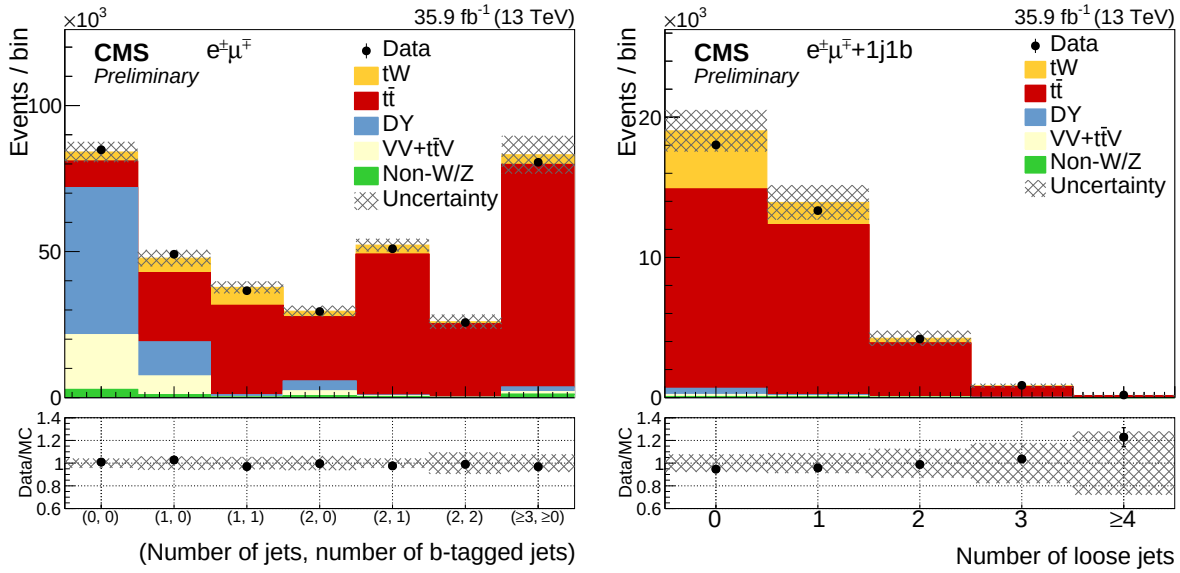

Figure 3: Left: yields observed in data, compared with those expected from simulation, as a function of the number of jets and number of b-tagged jets for events passing the baseline dilepton selection. The error band includes the statistical and all systematic uncertainties, except those from background normalization. Right: yields observed in data, compared with those expected from simulation, as a function of the number of loose jets for events passing the $e^{\pm}\mu^{\mp}$ selection in the 1j1b region. The hatched band includes the statistical and all systematic uncertainties. The bottom of the panel shows the ratio of data to the sum of the expected yields.

events in bin i and N_i^{bkg} is the number of expected background events in the same bin. In order to obtain the number of events after unfolding, a χ^2 minimization is obtained to solve Eq. (1). If needed, regularization terms are added to the χ^2 function in order to suppress unphysical fluctuations. In this note, the equation is solved using the implementation of `TUnfold` [44]. Since R matrices are found to be sufficiently well-conditioned, no regularisation is applied.

Afterwards, for each variable X, the absolute differential tW cross section for a given bin j at particle-level, $\left(\frac{d\sigma}{dX}\right)_j$, can be determined using the relation

$$\left(\frac{d\sigma}{dX}\right)_j = \frac{1}{\mathcal{L}} \frac{N_j^{sig,\,unf}}{\Delta_j}, \tag{2}$$

where Δ_j is the width of the bin j. The measurement is performed in a fiducial region defined by the same selection requirements employed in the event selection (see Table 1), described in Section 3, and applied on particle-level objects. The identification of particle-level objects is summarized in Table 2. These objects are constructed over stable (i.e. with a lifetime larger than 30 ps) generated particles following the conventions given in Ref. [45]. Muons and electrons not coming from hadron decays (prompt leptons) are dressed by taking into account the momenta of nearby photons within a $\Delta R<0.1$ cone. Jets are clustered from all stable particles excluding prompt electrons, prompt muons, prompt photons, and all neutrinos using the anti-k_T algorithm with a distance parameter of R=0.4. The information of the intermediate hadrons and τ leptons is used to know whether one jet is originated from a heavy-flavour quark (bottom or charm) or whether it arises as a decay product of a τ lepton.

Finally, the normalized differential cross sections are obtained by dividing the absolute differ-

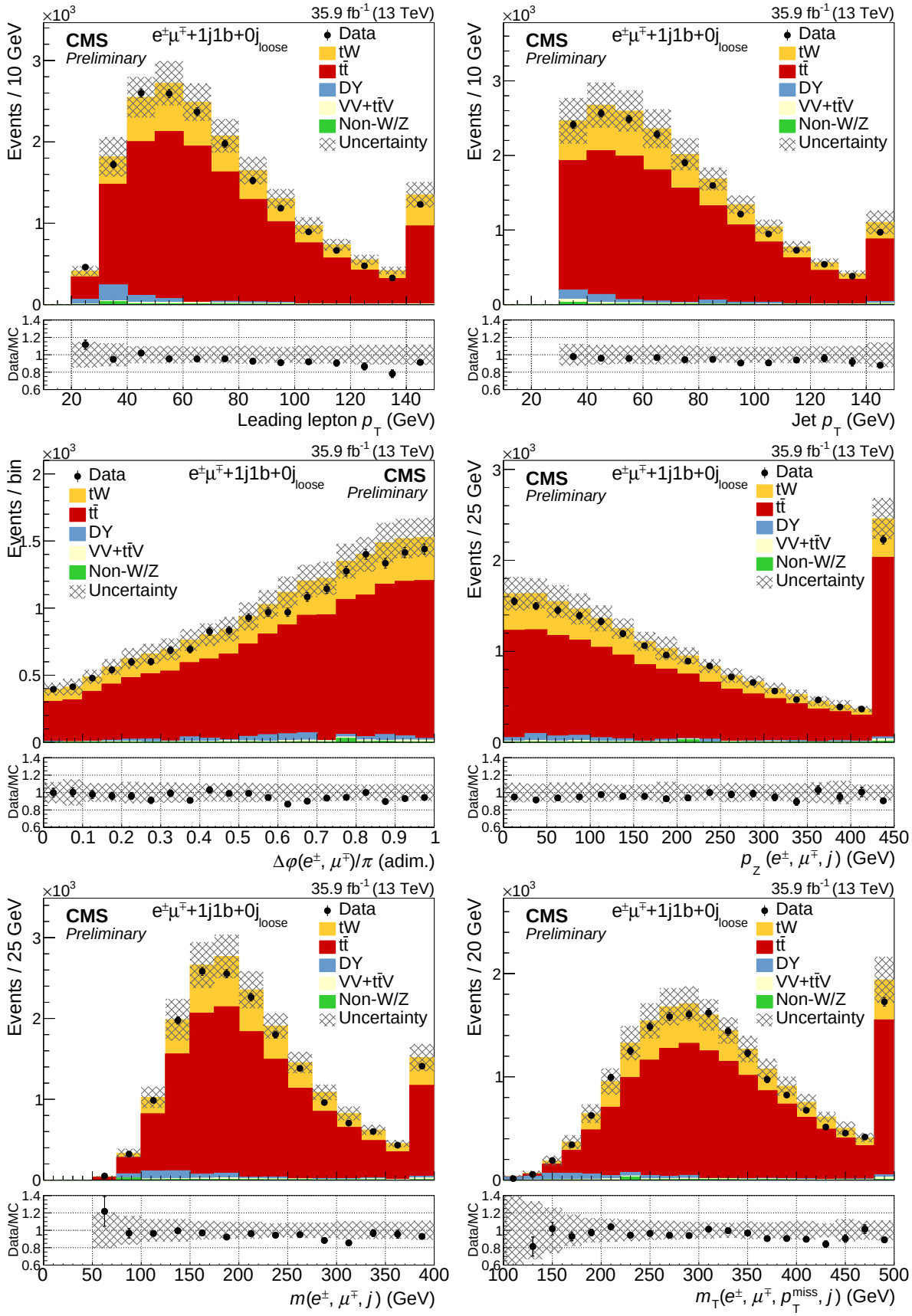

Figure 4: Yields observed in data, compared with those expected from simulation, as a function of different observables for the selected events. The hatched bands include the statistical and all systematic uncertainties. The last bin of each contribution contains overflow events. The bottom of each panel shows the ratios of data to the sum of the expected yields.

Table 1: Definition of the fiducial region.

Number of leptons	≥ 2
p_{T} (ℓ_1)	> 25 GeV
$m_{e\mu}$	> 20 GeV
Number of jets	1
Number of loose jets	0
Number of b jets	1

Table 2: Selection requirements of particle-level objects.

Muons		Electrons		Jets		Loose jets	
p_{T} (GeV)	$\lvert\eta\rvert$	p_{T} (GeV)	$\lvert\eta\rvert$	p_{T} (GeV)	$\lvert\eta\rvert$	p_{T} (GeV)	$\lvert\eta\rvert$
> 20	< 2.4	> 20	< 2.4 && (< 1.4442 || > 1.5660)	> 30	< 2.4	> 20 , < 30	< 2.4

ential cross section by the fiducial cross section (the sum over all bins of the differential cross section, σ_{fid}). This ratio allows the cancelation of several systematic uncertainties.

5 Systematic uncertainties

The measurement of the differential tW cross sections is affected by systematic uncertainties that originate from both detector effects and theoretical assumptions. Due to the dominating presence of $\mathrm{t\bar{t}}$ events in the signal region, the impact of these uncertainty sources is mainly produced by uncertainties in the $\mathrm{t\bar{t}}$ estimation. Uncertainties affecting the R matrix in the tW signal are relatively smaller.

Each source of systematic uncertainty is assessed individually either by suitable variations of the MC simulations or by variations of parameter values in the analysis within their estimated uncertainties. For each systematic uncertainty, the complete analysis procedure is done with the varied simulated sample. The difference between the nominal result and varied distribution is taken as the systematic uncertainty. In the case of one-sided uncertainties (jet energy resolution, top quark p_{T}), the same value is assigned before unfolding in the two directions.

5.1 Experimental uncertainties

Uncertainties originating from detector effects affect all processes involved. The final uncertainty is taken as the difference between the nominal result and the result obtained when varying the affected parameter by its uncertainty.

Jet energy scale and resolution The uncertainty due to the limited knowledge of the JES and jet energy resolution (JER) is determined by varying the scale and resolution within the uncertainties in bins of p_{T} and η, typically by a few percent [41]. The JES uncertainties are propagated to $\vec{p}_{\mathrm{T}}^{\,\mathrm{miss}}$.

b-tagging efficiency The uncertainties resulting from the b tagging efficiency and misidentification rate are assessed by varying, within their uncertainties, the b tagging data-to-simulation scale factors of the b jets and the light-flavor jets, respectively. These uncertainties vary with the p_{T} and η of the jet and amount to approximately 2% for b jets and 10% for mistagged jets [43], as determined in simulated $\mathrm{t\bar{t}}$ events.

Trigger and lepton identification The uncertainties in the trigger and lepton identification efficiencies in simulation are estimated by varying data-to-simulation scale factors by their uncertainties. These are about 0.7 and 1.5%, respectively, with some dependence on the lepton p_{T} and η.

Pileup The uncertainty assigned to the number of pileup events in simulation is obtained by changing the inelastic pp cross section, which is used to estimate the pileup in data, within its uncertainty of $\pm$4.6% [46].

Luminosity The uncertainty on the integrated luminosity is estimated to be 2.5% [47].

5.2 Modeling Uncertainties

The modeling of the $\mathrm{t\bar{t}}$ and tW events by the simulation is an important ingredient in this measurement. The impact of theoretical assumptions in the modeling is determined by repeating the analysis and replacing the nominal POWHEG $\mathrm{t\bar{t}}$ and/or tW simulation by dedicated simulation samples with altered parameters. The difference in the results is taken as the systematic uncertainty.

Matrix element (ME) scale The uncertainty in the modeling of the hard-production process is assessed by changing independently μ_{R} and μ_{F} in the POWHEG sample by factors of 2 and 0.5 relative to their common nominal value. This variation is performed separately for $\mathrm{t\bar{t}}$ and tW events.

Parton shower In order to take into account parton-shower (PS) uncertainties, different effects are studied:

- Underlying event: PYTHIA parameters that are tuned to the measurements of the underlying event [25, 26], to account for non-perturbative QCD effects, are varied up and down within their uncertainties in simulated $\mathrm{t\bar{t}}$ events.
- ME/PS matching: the uncertainty in the combination of the ME calculation with the parton shower in simulated $\mathrm{t\bar{t}}$ events is estimated from the variation, within its uncertainties, of the POWHEG parameter $h_{\mathrm{damp}} = 1.58^{+0.66}_{-0.59}\, m_{\mathrm{t}}$ [26], which regulates the damping of real emissions in the NLO calculation when matching to the PS [25].
- Initial- (final-) state radiation scale: the PS scale used for the simulation of the initial- (final-) state radiation is varied up and down by a factor of two. These variations are motivated by the uncertainties in the PS tuning [25]. This variation is performed simultaneously for $\mathrm{t\bar{t}}$ and tW events.
- Color reconnection: the effect of multiple parton interactions and the parameterization of color reconnection have been studied in Ref. [26] and are varied accordingly in simulated $\mathrm{t\bar{t}}$ events. In addition, we use a simulation including color reconnection of early resonant decays. The uncertainties that arise from ambiguities in modeling color-reconnection effects are estimated by comparing the default model in PYTHIA with two alternative models of color reconnection, a model with string formation beyond leading color [48] and a model in which the gluons can be moved to another string [49]. All models are tuned to measurements of the underlying event [25, 26]. The largest variation in each bin with respect to the nominal yield is taken as the systematic uncertainty.

PDF The uncertainty from the choice of PDFs is determined by reweighting the sample of simulated $t\bar{t}$ events according to the 100 NNPDF3.0 replicas [18]. For each bin, the root-mean-square of the variation in the acceptance for all the PDF sets is taken as an uncertainty.

Top quark mass The nominal top quark mass of 172.5 GeV is modified by ± 1 GeV in the simulation, which corresponds to twice the measured uncertainty by CMS [50]. The difference with respect to the nominal results is taken as the corresponding uncertainty.

Top quark p_T The uncertainty associated to the mismodeling of the momentum of the top quark is taken as the difference with respect to the uncorrected shapes.

5.3 Background normalization uncertainties

A normalization uncertainty of 4% [51] is used for $t\bar{t}$ events. For $t\bar{t}V$, VV, DY and non-W/Z background contributions, a conservative normalization uncertainty of $\pm 50\%$ is assumed, as done in Ref. [14].

6 Results

The normalized differential tW cross section as a function of the observables mentioned in Section 1 are shown in Figs. 5 and 6. Fair agreement, within the uncertainties, with the predictions from POWHEG DR, POWHEG DS and MADGRAPH5_aMC@NLO is observed. The main sources of systematic uncertainty in the measurement (and their relative effect) are also shown. In general, uncertainties coming from JES and JER are the dominant ones, because of their large effect in the background estimation.

7 Summary

The measurement of the normalized differential cross section of the production of a top quark in association with a W boson using $35.9\,\text{fb}^{-1}$ of data recorded by CMS has been presented for a final state containing an electron and a muon. The measurements are made as a function of various properties of the event: the transverse momentum of the leading lepton, the transverse momentum of the jet; the difference in the φ angle of the muon and the electron; the longitudinal momentum of the muon, the electron and the jet; the invariant mass of the muon, electron and the jet; and the transverse mass of the electron, the muon, the jet, and the missing transverse momentum. The main sources of uncertainty, both in the jet reconstruction and the theoretical modeling, are driven by the overwhelming $t\bar{t}$ background. The results obtained are, in general, consistent with the expectations from the two models used for the modeling of the tW signal, POWHEG and MADGRAPH5_aMC@NLO.

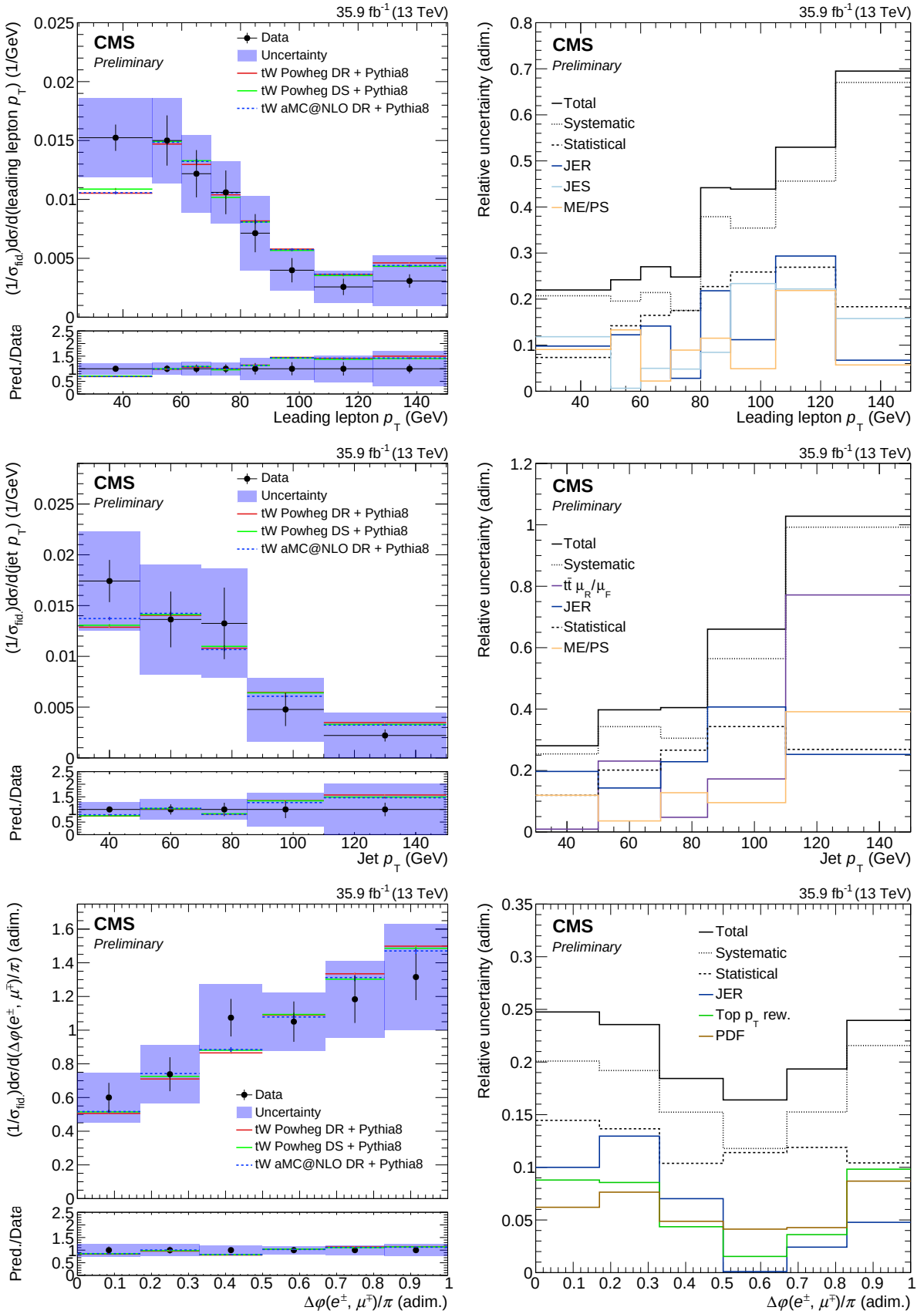

Figure 5: Left: normalized differential tW production cross section as a function of the p_{T} of the leading lepton (top), p_{T} of the jet (middle) and $\Delta\varphi(\mathrm{e}^{\pm},\mu^{\mp})$ (bottom). The solid band represents the total uncertainty. Predictions from POWHEG and MADGRAPH5_aMC@NLO are also shown. In the bottom panel, the ratio between predictions and data is shown. Right: total, systematic, statistical and individual leading (averaging over all bins) sources of uncertainty as a function of each observable.

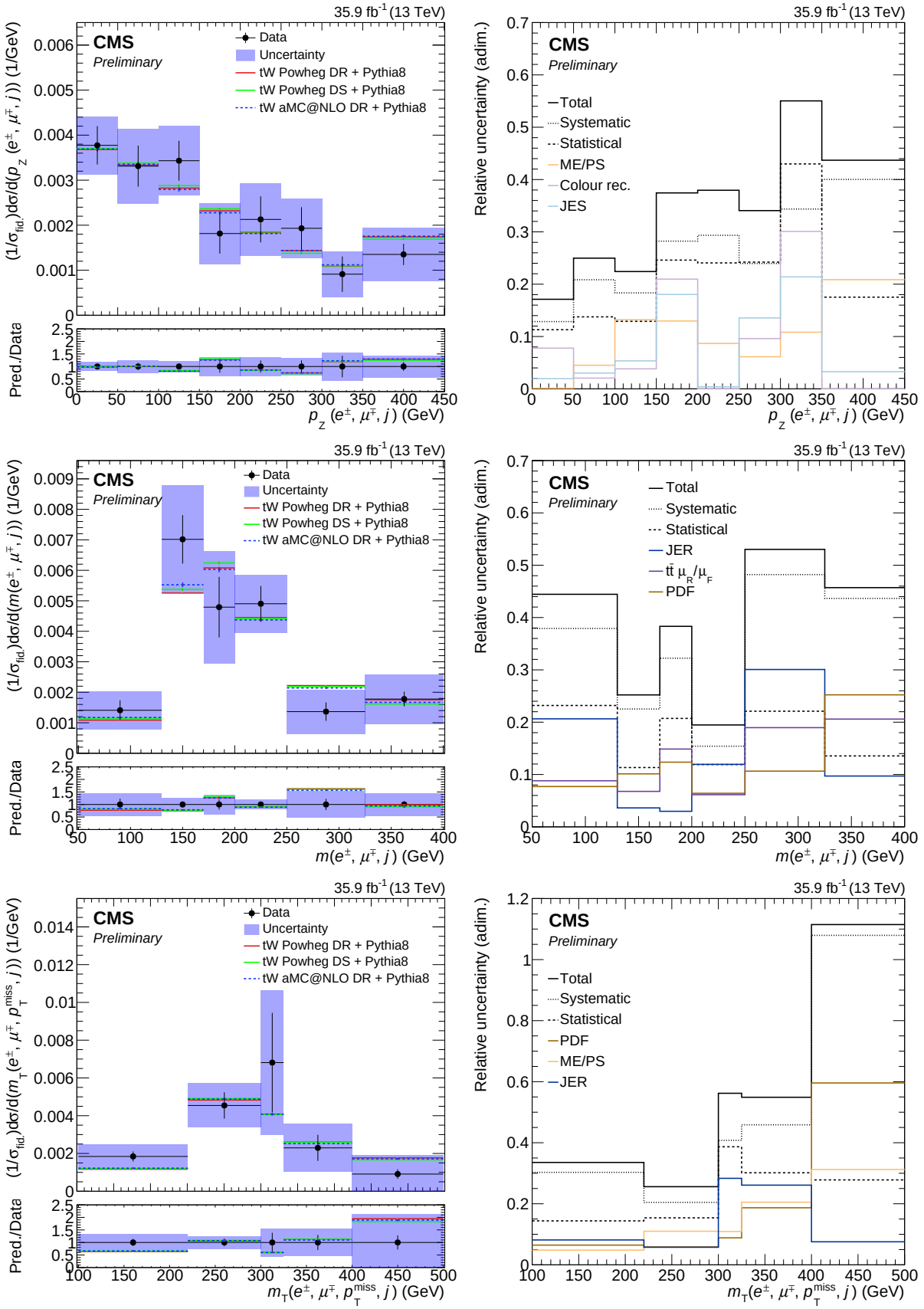

Figure 6: Left: normalized differential tW production cross section as a function of $p_{\mathrm{Z}}(\mathrm{e}^{\pm},\mu^{\mp},j)$ (top), $m(\mathrm{e}^{\pm},\mu^{\mp},j)$ (middle) and $m_{\mathrm{T}}(\mathrm{e}^{\pm},\mu^{\mp},j,p_{\mathrm{T}}^{\mathrm{miss}})$ (bottom). The solid band represents the total uncertainty. Predictions from POWHEG and MADGRAPH5_aMC@NLO are also shown. In the bottom panel, the ratio between predictions and data is shown. Right: total, systematic, statistical and individual leading (averaging over all bins) sources of uncertainty as a function of each observable.

References

[1] D0 Collaboration, "Observation of single top quark production", *Phys. Rev. Lett.* **103** (2009) 092001, doi:10.1103/PhysRevLett.103.092001, arXiv:0903.0850.

[2] CDF Collaboration, "First observation of electroweak single top quark production", *Phys. Rev. Lett.* **103** (2009) 092002, doi:10.1103/PhysRevLett.103.092002, arXiv:0903.0885.

[3] S. Frixione et al., "Single-top hadroproduction in association with a W boson", *JHEP* **07** (2008) 029, doi:10.1088/1126-6708/2008/07/029, arXiv:0805.3067.

[4] A. S. Belyaev, E. E. Boos, and L. V. Dudko, "Single top quark at future hadron colliders: Complete signal and background study", *Phys. Rev. D* **59** (1999) 075001, doi:10.1103/PhysRevD.59.075001, arXiv:hep-ph/9806332.

[5] C. D. White, S. Frixione, E. Laenen, and F. Maltoni, "Isolating Wt production at the LHC", *JHEP* **11** (2009) 074, doi:10.1088/1126-6708/2009/11/074, arXiv:0908.0631.

[6] T. M. P. Tait and C. P. Yuan, "Single top quark production as a window to physics beyond the standard model", *Phys. Rev. D* **63** (2000) 014018, doi:10.1103/PhysRevD.63.014018, arXiv:hep-ph/0007298.

[7] Q.-H. Cao, J. Wudka, and C. P. Yuan, "Search for new physics via single top production at the LHC", *Phys. Lett. B* **658** (2007) 50, doi:10.1016/j.physletb.2007.10.057, arXiv:0704.2809.

[8] V. Barger, M. McCaskey, and G. Shaughnessy, "Single top and Higgs associated production at the LHC", *Phys. Rev. D* **81** (2010) 034020, doi:10.1103/PhysRevD.81.034020, arXiv:0911.1556.

[9] N. Kidonakis, "Theoretical results for electroweak-boson and single-top production", in *Proceedings, 23rd International Workshop on Deep-Inelastic Scattering and Related Subjects (DIS 2015): Dallas, Texas, USA, April 27-May 01, 2015*, volume DIS2015, p. 170. 2015. arXiv:1506.04072.

[10] CMS Collaboration, "Evidence for associated production of a single top quark and W boson in pp collisions at $\sqrt{s} = 7$ TeV", *Phys. Rev. Lett.* **110** (2013) 022003, doi:10.1103/PhysRevLett.110.022003, arXiv:1209.3489.

[11] ATLAS Collaboration, "Evidence for the associated production of a W boson and a top quark in ATLAS at $\sqrt{s} = 7$ TeV", *Phys. Lett. B* **716** (2012) 142, doi:10.1016/j.physletb.2012.08.011, arXiv:1205.5764.

[12] CMS Collaboration, "Observation of the associated production of a single top quark and a W boson in pp collisions at $\sqrt{s} = 8$ TeV", *Phys. Rev. Lett.* **112** (2014) 231802, doi:10.1103/PhysRevLett.112.231802, arXiv:1401.2942.

[13] ATLAS Collaboration, "Measurement of the production cross-section of a single top quark in association with a W boson at 8 TeV with the ATLAS experiment", *JHEP* **01** (2016) 064, doi:10.1007/JHEP01(2016)064, arXiv:1510.03752.

[14] CMS Collaboration, "Measurement of the production cross section for single top quarks in association with W bosons in proton-proton collisions at $\sqrt{s} = 13$ TeV", *JHEP* **10** (2018) 117, doi:10.1007/JHEP10(2018)117, arXiv:1805.07399.

[15] ATLAS Collaboration, "Measurement of the cross-section for producing a W boson in association with a single top quark in pp collisions at $\sqrt{s} = 13$ TeV with ATLAS", *JHEP* **01** (2018) 063, doi:10.1007/JHEP01(2018)063, arXiv:1612.07231.

[16] ATLAS Collaboration, "Measurement of differential cross-sections of a single top quark produced in association with a W boson at $\sqrt{s} = 13$ TeV with ATLAS", *Eur. Phys. J. C* **78** (2018) 186, doi:10.1140/epjc/s10052-018-5649-8, arXiv:1712.01602.

[17] E. Re, "Single-top Wt-channel production matched with parton showers using the POWHEG method", *Eur. Phys. J. C* **71** (2011) 1547, doi:10.1140/epjc/s10052-011-1547-z, arXiv:1009.2450.

[18] NNPDF Collaboration, "Parton distributions for the LHC Run II", *JHEP* **04** (2015) 040, doi:10.1007/JHEP04(2015)040, arXiv:1410.8849.

[19] T. Sjöstrand et al., "An introduction to PYTHIA 8.2", *Comput. Phys. Commun.* **191** (2015) 159, doi:10.1016/j.cpc.2015.01.024, arXiv:1410.3012.

[20] T. M. P. Tait, "tW^- mode of single top quark production", *Phys. Rev. D* **61** (1999) 034001, doi:10.1103/PhysRevD.61.034001.

[21] J. Alwall et al., "The automated computation of tree-level and next-to-leading order differential cross sections, and their matching to parton shower simulations", *JHEP* **07** (2014) 079, doi:10.1007/JHEP07(2014)079, arXiv:1405.0301.

[22] S. Alioli, P. Nason, C. Oleari, and E. Re, "A general framework for implementing NLO calculations in shower Monte Carlo programs: the POWHEG BOX", *JHEP* **06** (2010) 043, doi:10.1007/JHEP06(2010)043, arXiv:1002.2581.

[23] R. Frederix and S. Frixione, "Merging meets matching in MC@NLO", *JHEP* **12** (2012) 061, doi:10.1007/JHEP12(2012)061, arXiv:1209.6215.

[24] CMS Collaboration, "Event generator tunes obtained from underlying event and multiparton scattering measurements", *Eur. Phys. J. C* **76** (2016) 155, doi:10.1140/epjc/s10052-016-3988-x, arXiv:1512.00815.

[25] P. Skands, S. Carrazza, and J. Rojo, "Tuning PYTHIA 8.1: the Monash 2013 Tune", *Eur. Phys. J. C* **74** (2014) 3024, doi:10.1140/epjc/s10052-014-3024-y, arXiv:1404.5630.

[26] CMS Collaboration, "Investigations of the impact of the parton shower tuning in Pythia 8 in the modelling of $\mathrm{t\bar{t}}$ at $\sqrt{s} = 8$ and 13 TeV", CMS Physics Analysis Summary CMS-PAS-TOP-16-021, CERN, 2016.

[27] Y. Li and F. Petriello, "Combining QCD and electroweak corrections to dilepton production in the framework of the FEWZ simulation code", *Phys. Rev. D* **86** (2012) 094034, doi:10.1103/PhysRevD.86.094034, arXiv:1208.5967.

[28] J. M. Campbell, R. K. Ellis, and C. Williams, "Vector boson pair production at the LHC", *JHEP* **07** (2011) 018, doi:10.1007/JHEP07(2011)018, arXiv:1105.0020.

[29] M. Czakon, P. Fiedler, and A. Mitov, "Total top-quark pair-production cross section at hadron colliders through $o(\alpha_S^4)$", *Phys. Rev. Lett.* **110** (2013) 252004, doi:10.1103/PhysRevLett.110.252004, arXiv:1303.6254.

[30] M. Czakon and A. Mitov, "Top++: A program for the calculation of the top-pair cross-section at hadron colliders", *Comput. Phys. Commun.* **185** (2014) 2930, doi:10.1016/j.cpc.2014.06.021, arXiv:1112.5675.

[31] CMS Collaboration, "Measurement of normalized differential $\mathrm{t\bar{t}}$ cross sections in the dilepton channel from pp collisions at $\sqrt{s} = 13$ TeV", *JHEP* **04** (2018) 060, doi:10.1007/JHEP04(2018)060, arXiv:1708.07638.

[32] CMS Collaboration, "Measurement of differential cross sections for top quark pair production using the lepton+jets final state in proton-proton collisions at 13 TeV", *Phys. Rev. D* **95** (2017) 092001, doi:10.1103/PhysRevD.95.092001, arXiv:1610.04191.

[33] CMS Collaboration, "Measurement of the differential cross section for $\mathrm{t\bar{t}}$ production in the dilepton final state at $\sqrt{s} = 13$ TeV", CMS Physics Analysis Summary CMS-PAS-TOP-16-011, CERN, 2016.

[34] CMS Collaboration, "Measurement of the differential cross section for top quark pair production in pp collisions at $\sqrt{s} = 8$ TeV", *Eur. Phys. J. C* **75** (2015) 542, doi:10.1140/epjc/s10052-015-3709-x, arXiv:1505.04480.

[35] CMS Collaboration, "Measurement of the $\mathrm{t\bar{t}}$ production cross section in the all-jets final state in pp collisions at $\sqrt{s} = 8$ TeV", *Eur. Phys. J. C* **76** (2016) 128, doi:10.1140/epjc/s10052-016-3956-5, arXiv:1509.06076.

[36] CMS Collaboration, "Particle-flow reconstruction and global event description with the CMS detector", *JINST* **12** (2017) P10003, doi:10.1088/1748-0221/12/10/P10003, arXiv:1706.04965.

[37] CMS Collaboration, "Performance of electron reconstruction and selection with the CMS detector in proton-proton collisions at $\sqrt{s} = 8$ TeV", *JINST* **10** (2015) P06005, doi:10.1088/1748-0221/10/06/P06005, arXiv:1502.02701.

[38] CMS Collaboration, "Performance of the CMS muon detector and muon reconstruction with proton-proton collisions at $\sqrt{s} = 13$ TeV", *JINST* **13** (2018) P06015, doi:10.1088/1748-0221/13/06/P06015, arXiv:1804.04528.

[39] M. Cacciari, G. P. Salam, and G. Soyez, "The anti-k_{T} jet clustering algorithm", *JHEP* **04** (2008) 063, doi:10.1088/1126-6708/2008/04/063, arXiv:0802.1189.

[40] M. Cacciari, G. P. Salam, and G. Soyez, "FastJet user manual", *Eur. Phys. J. C* **72** (2012) 1896, doi:10.1140/epjc/s10052-012-1896-2, arXiv:1111.6097.

[41] CMS Collaboration, "Jet algorithms performance in 13 TeV data", CMS Physics Analysis Summary CMS-PAS-JME-16-003, CERN, 2017.

[42] CMS Collaboration, "Performance of missing energy reconstruction in $\sqrt{s} = 13$ TeV pp collision data using the CMS detector", CMS Physics Analysis Summary CMS-PAS-JME-16-004, CERN, 2016.

[43] CMS Collaboration, "Identification of heavy-flavour jets with the CMS detector in pp collisions at 13 TeV", *JINST* **13** (2018) P05011, doi:10.1088/1748-0221/13/05/P05011, arXiv:1712.07158.

[44] S. Schmitt, "TUnfold: an algorithm for correcting migration effects in high energy physics", *JINST* **7** (2012) T10003, doi:10.1088/1748-0221/7/10/T10003, arXiv:1205.6201.

[45] CMS Collaboration, "Object definitions for top quark analyses at the particle level", Technical Report CMS-NOTE-2017-004, CERN, Geneva, 2017.

[46] ATLAS Collaboration, "Measurement of the inelastic proton-proton cross section at $\sqrt{s} = 13$ TeV with the ATLAS detector at the LHC", *Phys. Rev. Lett.* **117** (2016) 182002, doi:10.1103/PhysRevLett.117.182002, arXiv:1606.02625.

[47] CMS Collaboration, "CMS luminosity measurements for the 2016 data taking period", CMS Physics Analysis Summary CMS-PAS-LUM-17-001, CERN, 2017.

[48] J. R. Christiansen and P. Z. Skands, "String formation beyond leading colour", *JHEP* **08** (2015) 003, doi:10.1007/JHEP08(2015)003, arXiv:1505.01681.

[49] S. Argyropoulos and T. Sjöstrand, "Effects of color reconnection on $\mathrm{t\bar{t}}$ final states at the LHC", *JHEP* **11** (2014) 043, doi:10.1007/JHEP11(2014)043, arXiv:1407.6653.

[50] CMS Collaboration, "Measurement of the top quark mass using proton-proton data at $\sqrt{s}$ = 7 and 8 TeV", *Phys. Rev. D* **93** (2016) 072004, doi:10.1103/PhysRevD.93.072004, arXiv:1509.04044.

[51] CMS Collaboration, "Measurement of the $\mathrm{t\bar{t}}$ production cross section, the top quark mass, and the strong coupling constant using dilepton events in pp collisions at $\sqrt{s} = 13$ TeV", *Eur. Phys. J. C* **79** (2019) 368, doi:10.1140/epjc/s10052-019-6863-8, arXiv:1812.10505.